UNCLASSIFIED

AD 401 759

Reproduced
by the

DEFENSE DOCUMENTATION CENTER

FOR

SCIENTIFIC AND TECHNICAL INFORMATION

CAMERON STATION, ALEXANDRIA, VIRGINIA

63 3 2

APGC-TDR-63-22

Study of Target Penetration Prediction by High Speed and Ultra High Speed Ballistic Impact

Final Report 1 July 1961-28 February 1963

APGC Technical Documentary Report No. APGC-TDR-63-22

APRIL 1963 ● OAR Project 9860

DEPUTY FOR AEROSPACE SYSTEMS TEST

AIR PROVING GROUND CENTER

AIR FORCE SYSTEMS COMMAND ● UNITED STATES AIR FORCE

EGLIN AIR FORCE BASE, FLORIDA

FOREWORD

This report was prepared under Air Force Contract Number AF 08(635)-2155, "Study of Target Penetration Prediction By High Speed and Ultra High Speed Ballistic Impact". Work was administered under the direction of APGC (PGTWR), Eglin Air Force Base, Florida, with Mr. A. G. Bilek as Project Engineer.

ABSTRACT

On the basis of a statistical study of existing experimental data relative to ballistic impact, engineering formulae were developed which will predict with an accuracy of 90%,

      (a) the depth of penetration

      (b) the volume of the crater

in semi-infinite targets of common metals over a wide range of impact velocities. The application of these equations in predicting the size and velocity of projectiles impacting orbital structures is also indicated.

A semi-rational penetration expression was developed from a work-energy consideration which suggests that the nonrecoverable target compression and shear strain energies may account for most of the kinetic energy of the projectile. This dimensional model agrees quite well with the general features of, and is subject to, the same limitations as existing theoretical and empirical models.

PUBLICATION REVIEW

This technical documentary report has been reviewed and is approved.

MORRILL E. MARSTON
Colonel, USAF
Deputy for Aerospace Systems Test

iii

TABLE OF CONTENTS

LIST OF SYMBOLS

A, B	-	constants (Eq. 21)
a,b,d,f,h,j,l	-	constants
C	-	series of constants as C_1, C_2, . . .
c	-	dilatational wave velocity
D_p	-	projectile diameter
E	-	energy
E_p	-	impact kinetic energy of projectile
e	-	tensile elongation (strain) at fracture (%)
F	-	target resistance force
G	-	modulus of rigidity
g	-	shear strain at fracture (%)
H	-	Brinell hardness
K	-	bulk modulus
k	-	constant
m	-	mass
P_c	-	crater depth measured from original target surface
p	-	pressure
r	-	radius
S	-	shear strength
T	-	target temperature
t	-	time
U	-	ultimate strength (tensile)
u	-	shock velocity

V	- volume
V_c	- crater volume below original target surface
v	- velocity, impact velocity
Y	- yield point or yield strength
γ	- shear strain
ν	- Poisson's ratio
ρ	- mass density
τ	- shear stress

SUBSCRIPTS

B	- backsplash
c	- crater
i	- interface between projectile and target
p	- projectile
pr.	- pressure
S	- denotes material strain, as E_S (strain energy)
t	- target
O	- denotes undisturbed condition (ahead of shock)
1	- denotes compressed condition (behind shock)
1,2,3. . .	- used with constants

INTRODUCTION

With the advent of ballistic missiles, satellites, and space vehicles a great deal of attention has understandably been centered about hypervelocity terminal ballistics. The velocity of meteorites varies from 11.2 to 72 km./sec. At a velocity of 50 km./sec., for example, a gram of material would have a kinetic energy equal to the potential energy of 360 grams of TNT. Therefore, meteoric material presents one of the greatest natural hazards to which satellites and space vehicles may be subjected. In addition, artificial "meteorites" with high relative kinetic energies appear attractive as anti ICBM defensive weapons.

The highest velocity discreet particles so far reported in terminal ballistic studies are 9 km./sec. fragments from shaped charges. Not only does a large gap exist between present experimental techniques and the maximum velocity of meteoric material, but the terminal ballistics of projectiles traveling less than 9 km./sec. are poorly understood.

The purpose of this study is to gather and assemble existing data on ballistic impact and on material failure, especially at high impact velocities or large loading - to establish the relative importance of such factors as projectile velocity, mass, projectile-target strengths, ductilities, densities, compressibilities, etc., and to use this information to deduce the approximate mathematical relationships of critical factors as the target structure responds to impact and is penetrated.

GENERAL ASPECTS OF TARGET BEHAVIOR

From an engineering point of view, the behavior of a target under
ballistic impact might be separated into three categories ... penetration,
penetration-plus-scabbing, and perforation. Scabbing, of course, is just
one phenomenon of tensile fracture resulting from stress wave interference.
In addition to tension (or compression) the targets are subject to shear,
but in each case the resulting fracture can usually be attributed to tran-
sient stress conditions that develop as a result of stress wave interferences.
Some materials (steels) exhibit a time delay before the initiation of plas-
tic flow which tends to produce a more brittle type of fracture, while
other metals (aluminum, brass) do not show these time-dependent plastic
flow properties. Although there are a multiplicity of factors which may
affect target behavior, the factors that determine which of the three
behavior categories will result for a given set of impact conditions and
materials are principally the target thickness and whether the target
material behaves substantially as a brittle or ductile material.

The problem of predicting material resistance to high speed impact
is difficult largely because the question of ductility versus brittleness
is a relative and variable one. While some materials are more brittle or
ductile than others for a given set of conditions, a particular material
may behave in a brittle or ductile fashion depending on such conditions
as temperature, strain rate, and pressure. In general, a particular
material tends to become less ductile at higher strain rates and lower
temperatures and more ductile under high pressures. There is, at least
for ferrous metals, a definite transition temperature range separating
brittle and ductile behavior. Rapid strain rates tend to raise this
transition temperature range so that decidedly brittle behavior occurs
at higher temperatures when subjected to higher strain rates. This transi-
tion range is not generally found among non-ferrous metals.

DISCUSSION OF CRATER PARAMETERS

Metal targets tend to pass from "penetration" to "penetration-plus-
scabbing" to "perforation" types of behavior as the target thickness
decreases. However, the mechanism of these different behaviors and their
transition from one to the other are quite different in brittle and ductile
targets. A relatively thick ductile target will, in general, undergo a
more or less hemispherical crater formation under hypervelocity ballistic
impact. In this case, the depth of penetration and the crater volume would
assume equal status as the design variable dependent on several different
impact and material parameters. The mechanism of crater formation in a
thick brittle target is somewhat different in that the brittle target may
tend to spall in the vicinity of the crater rim and is more susceptible
to scabbing fracture. Since the energy necessary to propagate a crack

is quite small, it seems reasonable that spall may have a primary effect on crater volume, but only a secondary effect on penetration. An example of this secondary effect on penetration would be that the spalled away material might give a larger solid angle for the low resistance ejection of material from the growing crater. As long as the impact velocity is high enough, it might appear that depth of penetration into thick targets would be less sensitive to the ductility of the target than would crater volume.

DISCUSSION OF MATERIAL PARAMETERS

For given projectile and target geometry and impact conditions, target behavior is a function of the pertinent material properties that are operative under the prevailing impact conditions, which include high pressures, high strain rates and possible high or low ambient target temperatures. Since the fundamental material properties used in this study, of necessity, refer to conditions which are greatly different from those under hypervelocity impact loading, some justification, or at least discussion, of the adequacy of their use is required.

The projectile and target material properties used in the study include densities under normal pressures and temperatures, and mechanical properties under static or quasi-static loading. With the exception of shear strength and Brinell hardness, all of the mechanical properties used are tensile properties.

While it is well known that material behavior changes radically under conditions of high pressure, high strain rate and large temperature changes, it is believed that the properties used in this study are, generally speaking, indicative of the behavior under conditions of high speed impact. That is, higher strain rates generally produce greater material strengths, less compressibility and less ductility. Temperature decreases, in general, have similar effects on material strength, compressibility and ductility. Also decreasing temperatures generally increase material hardness. With regard to high and low target temperatures, it appears that high ambient target temperatures (below the melting point of the material) are probably not as important as low temperature effects, since material behavior at higher temperatures usually takes the form of a delayed creep or flow, which would not seem to be pronounced under very rapid transient loads. High pressures generally increase material strength, ductility and hardness, and decrease compressibility. The use, in a comparative manner, of the more accurately defined static and low strain rate material properties seems to be further justified in light of the knowledge that many factors such as thermal effects and modification of the crystalline structure of the target material by transient stress waves may have a decided influence on behavior, apart from the mechanical properties of the target material, and factors such as these are little understood or difficult to evaluate.

3

The following is a summary of the general effects of increased strain rates and pressures and decreased temperatures on material behavior:

	Increased Strain Rate	Decreased Temp.	Increased Press.
Strength (Generally)	Greater	Greater	Greater
Compressibility (Generally)	Less	Less	Less
Ductility (Generally)	Less	Less	Greater
Brinell Hardness	----	Greater	Greater

The Brinell definition of hardness is specified since hardness is defined in various ways, some of which may not follow this general behavior (for example, when defined as energy absorbing capacity).

The previous discussion has summarized a few of the more pertinent aspects of material behavior under conditions which, for low temperatures, probably approximate those found in the hypervelocity impact of a meteoric particle with a space vehicle. However, our experimental information on the effect of high strain rates and high pressures on fundamental material behavior falls far short of those experienced in hypervelocity impact loading. Also, it would be foolhardy not to expect that some contradictions to the above general rules exist. For example, certain grades of mild steel are known to have a so-called "brittle range" under static loading (ordinary room temperature to about 500 degrees Fahrenheit) where an increase in temperature is accompanied by an increase in strength and brittleness. This, however, is abnormal when compared with other temperature ranges for the same material and is not found at all in most other metals.

Bjork[6] has pointed out an apparent inconsistency in relative material compressibility under high pressures as compared with low pressures, although it does not violate the general statement that compressibility decreases with pressure. He showed that the hugoniots for some metals tend to "cross over". Specifically, the graphs of pressure versus relative density (ρ/ρ_0) for lead and aluminum cross. At low pressures aluminum is more resistant to density change than lead, but at high pressures this is reversed. While a theoretical study of the mechanics of impact behavior must necessarily consider the hugoniots, it is probable that in a statistical study this effect can be assumed to be reflected generally in the relative material densities, strengths, compressibilities, etc. The important fact in this regard seems to be that the hugoniots for different materials have the same general shape and that compressibility generally decreases with increased pressure.

EMPIRICAL MODEL

Approximately 1800 experimental data points have been accumulated from the original papers of many investigators and analyzed during the course of this study. Most of the accumulated data (with the major exception of the higher velocity shots, especially in aluminum) have been compiled and analyzed by Bruce[31] or Herrmann and Jones[9]. Of the 1800 shots only about half have proven really useful and there are many discrepancies among these useful shots. The majority of shots were eliminated for two reasons: (1) failure of the investigator to adequately specify the material of the target, and (2) the large divergence of some impact data from other data taken by other investigators into the same materials under very similar impact conditions. Many experimentors have chosen to present their data only on curves and graphs rather than in tables of raw data, thus increasing the chance of recording and reading errors.

It was decided to relate the dependent variables (penetration depth and crater volume in semi-infinite* targets) to the independent variables through a simple power law. No additional assumptions were made regarding the process of ballistic impact or the shape of the craters formed. The analysis has produced engineering equations which will predict, within the limits of the data, the penetration depth and crater volume in common metallic targets with an accuracy of about 90%. By the very manner in which experimental data must be gathered and crater parameters must be measured, it is doubtful that the reproducibility of the original data is greater than 90%.

PRELIMINARY EMPIRICAL ANALYSIS OF P_c

A preliminary analysis was performed on data compiled prior to December, 1961 was reported in the Second[2] and Third[3] Quarterly Reports. Since the distribution of target materials as a function of velocity was quite biased, the detailed results of this preliminary analysis are not very useful. It was performed more to establish methods for later analyses and the detailed results will not be reproduced in this report.

Penetration depth was considered a function of ten independent variables according to the equation

$$P_c = k_0 \, v^{k_1} \, \rho_t^{k_2} \, \rho_p^{k_3} \, V_p^{k_4} \, T^{k_5} \, Y_t^{k_6} \, Y_p^{k_7} \, c_t^{k_8} \, U_t^{k_9} \, D_p^{k_{10}} \, .$$

---

*Semi-infinite according to the rule-of-thumb published by Kinard, et al[7], that the penetration is no greater than 20% of the target thickness

This equation was reduced to its associated linear form

$$\log P_c = \log k_0 + k_1 \log v + \ldots\ldots\ldots\ldots + k_{10} \log D_p$$

and the method of least squares was used to determine a "best" set of values for the variable exponents (coefficients) k_i based on minimizing the value of

$$\sum_{i=0}^{10} \left[\log (P_c)_{experimental} - \log (P_c)_{calculated}\right]^2 .$$

The independent variables were dropped one-by-one starting with D_p and the effect on the k_i was noted.

After the k_i were computed, various statistical tests were made to determine the validity of the results obtained. The per cent of the variance in the log of dependent variable (P_c) that is explained by the logs of the independent variables is given by the multiple correlation coefficient. These multiple correlation coefficients were calculated after each independent variable was dropped. An analysis of this variance, using the F distribution, tests the null hypothesis that all β_i are zero. Separate tests of the individual hypothesis $\beta_i = 0$ were made using the t distribution. Variables corresponding to the β_i that were not significant by the preceding test were then removed and separate tests were made on each of the removed variables to see whether the adding of this variable improved the fit. Individual correlation coefficients between all independent variables were also calculated.

The significance of the target yield strength above many of the other variables contributing to the multiple correlation coefficients was noted. However, the target yield strength (Y_t), the dilatational wave velocity in the target (c_t), and the target ultimate strength (U_t) are statistically indistinguishable as evidenced by the fact that the calculated individual correlation between them is over 95%. The diameter of the projectile (D_p) is also statistically indistinguishable from the volume of the projectile (V_p) so that the effect of dropping (D_p) was insignificant. With the exception of the above correlations and the dependence of c_t on ρ_t, the rest of the individual correlation coefficients showed a low degree of interdependence.

The preliminary analysis was made on approximately 1200 experimental shots only half of which were reported in enough detail to enable assignment of strength parameters to the target and projectile. Of the resulting 600 shots, only 174 were performed at velocities greater than the bulk wave velocity in the target medium and over 90% of these "supersonic" shots were in lead targets where the bulk wave velocity is quite low (about 5400 feet per second). This analysis, then, seemed to indicate that the crater depth

could be adequately predicted on the basis of 4 or 5 out of the ten independent variables chosen, at least for impact velocities below the bulk or dilatational wave velocity in the target medium.

ANALYSIS OF P_c/D_p

An analysis of the penetration depth in semi-infinite targets divided by the diameter of the projectile (P_c/D_p) was performed on 1,270 shots which were reported in enough detail to assign strength parameters to the target materials. The experimental data was divided into two parts: (1) those having impact velocities below v_3 (Hopkins and Kolsky[8]), and (2) those with impact velocities near or above v_3, where

$$v_3 = \sqrt{K_t/\rho_t}$$

The distribution of target materials as a function of impact velocity is given in Figure 1* for the "low" velocity set (985 shots). Since a large number of recording errors were discovered in the high velocity data, the results of this run (recorded in the Fourth Quarterly Report[4]) have been eliminated from the present report.

As was done in the previous analysis of (P_c), (P_c/D_p) was fitted to a simple power law formula

$$P_c/D_p = k_o v^{k_1} \rho_t^{k_2} \rho_p^{k_3} \cdots\cdots$$

with no additional assumptions being made. This equation was then reduced to its associated linear form

$$\log P_c/D_p = \log k_o + k_1 \log v + k_2 \log \rho_t + \cdots\cdots$$

and the method of least squares was used to determine a "best" set of values for the variable exponents (coefficients) k_i based on minimizing the value

$$\sum_{i=0}^{n} \left[\log (P_c/D_p)_{experimental} - \log (P_c/D_p)_{calculated} \right]^2$$

The independent variables were dropped one-by-one, starting with the last, and the effect on the remaining k_i determined. These are summarized for

* Appendix B

7

the low velocity data in Tables I, II, III and IV, which appear in Appendix B.

After the k_1 were computed, the usual statistical tests were made to determine the validity of the results. The per cent of variance in log P_c/D_p that is explained by the variation in the logs of the independent variables is given by the multiple correlation coefficients listed in each table. Individual correlation coefficients between all variables were also computed on the low velocity shots. These results appear as Table V, also in Appendix B.

From Table V, it may be seen that the close correlation between the dilatational wave velocity (c_t), the ultimate strength (U_t), the shear strength (S_t), the Brinell hardness (H_t), and the yield strength (Y_t) render these independent variables statistically indistinguishable. In addition, the correlation coefficient between the bulk modulus (K_t) and each of the above variables is greater than 0.50. Any of the empirical power law equations containing more than one of these closely correlated variables is likely to be completely misleading in the coefficients (exponents) of the correlated variables. All the rest of the variables including the per cent elongation (e_t) were statistically independent.

ANALYSIS OF $P_c/V_p^{1/3}$

For this analysis, the cube root of the projectile volume was used to render the penetration non-dimensional. This not only makes the results of the empirical analysis assume the same form as the results of the Dimensional Model which follows, but also eliminates the ambiguity involved in defining the projectile diameter when the projectile is not exactly spherical.

Before this analysis was run, elaborate steps were taken to "clean up" the accumulated experimental data. First, the "high" velocity data were completely rechecked for recording errors and shots at other than normal impact angles were eliminated. The body of "low" velocity data, being much larger, was checked on the computer. The equation from Table III,

$$P_c/_{D_p} = 8.43 \times 10^{-3} v^{1.06} \rho_t^{-.365} \rho_p^{.984} S_t^{.400} T_t^{.586} e_t^{.010} V_p^{.035} c_t^{.252}$$

which yielded a multiple correlation coefficient of 0.846 on the previous analysis, was used to calculate the depth of penetration from the independent variables of each of the "low" velocity shots. The calculated penetration depth was then compared with the experimental penetration depth and a per cent error was computed for each shot. All data points with an error of greater than 50% were then scrutinized for recording or computer errors.

8

Shots which showed a large deviation and whose values had been read from curves rather than tables in the original papers were immediately eliminated. Other shots, which did not seem to fit with the rest of the experimental data taken from their particular source were also eliminated. Many shots with errors greater than 50% were deemed correct and were left in. Finally, the small number of shots in which the target temperature or the impact angle were other than ambient and $90°$, respectively, were eliminated.

After "cleaning", a total of 1008 shots remained ..... 742 classified as "low" velocity and 266 classified as "high" velocity. The distributions of target materials as a function of impact velocity for each of these compilations are shown in Figures 2 and 3 of Appendix B.

The "low" velocity and the "high" velocity data were individually fit to the simple power law formula in the form

$$P_{c/V_p^{1/3}} = k_o \, v^{k_1} \, \rho_t^{k_2} \, \rho_p^{k_3} \quad .....$$

with the digital computer programmed to calculate least squares values of the k_i and the multiple correlation coefficients between the dependent variable and all of the independent variables taken together. As was done in the previous runs, the k_i were dropped one by one and the effect on the multiple correlation coefficient was noted. The product of the shear strength and the per cent elongation (Se) was used as one of the variables in this analysis because of its appearance in the Dimensional Model which follows. The results of eight separate runs appear in Appendix B ....., Tables VI, VII, VIII, and IX for the "low" velocity data and Tables X, XI, XII, and XIII for the "high" velocity data.

The multiple correlation coefficients in Tables 1 - 8 show that using four independent variables (i.e., $v, \rho_p, S_t,$ and ρ_t) it is possible to explain 92% of the variation in penetration depth using the low velocity data and 87% of the variation in penetration depth using the high velocity data.

ANALYSIS OF V_c/E_p

Finally, the ratio of crater volume to kinetic energy was used as the dependent variable in the equation

$$V_{c/E_p} = k_o \, v^{k_1} \, \rho_p^{k_2} \, S_t^{k_3} \, \rho_t^{k_4} \quad .$$

As usual, the k_i were found by the method of least squares. Since it had been well established by this time that only four independent variables (including a strength parameter) are necessary to adequately describe the penetration, the variables were not dropped one by one. The "low" (Fig. 2)

9

and "high" (Fig. 3) velocity data were substituted separately. Because the crater volume was not measured on all data points for which the penetration depth was obtained, only 543 "low" velocity shots and 220 "high" velocity shots contributed to this analysis. The results appear in Table XV of Appendix B.

QUALITATIVE DISCUSSION OF THE EMPIRICAL MODEL

Reference to Figures 2 and 3 in Appendix B shows that the "low" velocity shots are fairly well distributed among target materials. Each bar on Figure 2 represents the total number of shots over a velocity range of one thousand feet per second while each bar on Figure 3 represents a range of two thousand feet per second. The relatively large number of shots into lead, copper, and 2024 T4 aluminum represent soft, medium, and fairly hard materials, respectively. Figure 3 shows a very large peak from 1000 to 5000 feet per second, but any attempt to flatten the distribution as a function of velocity would have meant the elimination of a tremendous number of shots with a consequent decrease in the statistical confidence. Figure 3 points out a definite need for experimental data over the velocity range of 17,000 to 27,000 feet per second. Light gas guns have been developed with muzzle velocities up to 25,000 feet per second, but so far no cratering data has appeared in the literature at these high velocities. The experiments conducted at velocities above 25,000 feet per second all employed shaped charge techniques (Aerojet General for the Terminal Ballistic Division at Eglin AFB, Florida). It would be nice to see more impacts into other than 2023 T4 targets. Finally, there is a need for data at much higher velocities.

In practically all of the data used in this empirical study, the projectile shape is spherical or near-spherical (i.e., cylinder with $l/D = 1$ or fragment). At lower impact velocities there is no doubt that the shape of the projectile has a pronounced influence on cratering. As the impact velocity increases, it would seem reasonable to assume that the shape of the projectile becomes less and less important. However, over the velocity range considered in this study one would still expect the length to diameter ratio (l/D) of the projectile to have some effect. Until some high impact velocity (possibly equal to the sum of the dilatational wave velocity in the projectile and target materials) is reached, it will be possible for the tail of a projectile to be aware that something has happened to the head. Little experimental work has been done with high l/D ratios and it is not likely that any will appear for very high velocities. It is difficult enough to obtain a discreet projectile at very high velocities, let alone control its shape. Shaped charge jets might approximate high l/D ratio projectiles were it not for the fact that the jet is moving with nonuniform velocity along its length. Fortunately, from a practical standpoint, it is quite unlikely that space debris will appear in the form of long needles.

The fact that the multiple correlation coefficients for the "high" velocity data (Tables X through XIII) are somewhat lower than those for

the "low" velocity data (Tables VI through IX) might have been anticipated. Higher impact velocities become increasingly more difficult to measure accurately. In addition, the mass of the projectile in the shaped charge experiments (all above 25,000 feet per second) was determined from orthogonal photographs. For these and other reasons the higher velocity data is less reproducible than the lower velocity data.

It might be inferred from the results of this study that as long as four independent variables (v, ρ_p, ρ_t, plus one "strength" parameter) are used in the prediction formula, increasing the number of independent variables has little effect on the correlation. This is not true. As pointed out earlier in connection with Table V, all of the mechanical properties used in this study seem to have high correlation with one another. One would not expect the addition of variables highly correlated with existing variables to improve the multiple correlation. Target temperature was used as a variable in the analysis of P_c and P_c/D_p, but the number of shots in which the target temperature varied was so small, relative to the total number of shots, that dropping the temperature as a variable had little effect on the multiple correlation coefficient. Likewise, impact angle was not used as a variable due to the small number of shots at impact angles other than 90°.

It is interesting to note that the "low" velocity data indicate a dependence of cratering on the first power of the impact velocity. This linear dependence of (P_c) on (v) agrees with the discussion of the simple power law

$$P_c = k \, v^n$$

by Herrmann and Jones[9] in which they find that the experimental data, at least for aluminum, fits n = 1 over the approximate velocity of 7500 to 12,000 feet per second. They also point out that in the velocity range of 10,000 to 20,000 feet per second penetration may be approximated by the above equation with n = 2/3, and from 30,000 to 200,000 it may be approximated with n = 1/3. This type of high velocity behavior seems to be supported by the fact that the "high" velocity data (Tables X through XIII) indicate a dependence of ($P_c/V_p^{1/3}$) on a power of (v) somewhat less than 1/2. It might also be said that the decreasing power of ρ_p as velocity increases indicates that the data is approaching, but has not reached, the velocity regime in which Bjork's hydrodynamic theory subtends.

The low velocity data also seem to indicate a dependence of (P_c/D_p) or ($P_c/V_p^{1/3}$) on the first power of the projectile density (ρ_p). This, coupled with the linear dependence on velocity mentioned above, fits Herrmann and Jones' assumption of a resistive force dependent on velocity as

$$F = k \, D_p^2 \, v$$

which leads to a penetration expression of the form

$$P_c/D_p = k\, \rho_p\, v$$

where k is a constant. As they point out, an equation somewhat like the above can be used to fit low velocity impact data.

The high velocity data show a dependence of $(P_c/V_p^{1/3})$ on ρ_p to a power of about 2/3. This is a definite disagreement with the widely used empirical expression

$$P_c/V_p^{1/3} = k\, v^{2/3}\, \rho_p^{1/3}$$

which is obtained from the observation[12, 13, 14, 15, 16, 17, 18, 19, 20] that the crater volume is proportional to the kinetic energy, coupled with the observation [15, 16, 19, 20, 21, 22] that the craters formed are hemispherical. Palmer[10] points out that all Utah cratering studies seem to best fit an equation similar to the above equation in which the exponent of ρ_p is 1/2.

Both the "high" and "low" velocity data point to a real dependence of cratering on at least one target "strength" parameter. The "low" velocity data (Tables VI, VIII, and IX) favor an inverse dependence of $(P_c/V_p^{1/3})$ on S_t, H_t, or $(Se)_t$ to a power slightly more than 1/3 while the "high" velocity data (Tables X, XII, XIII) favor an inverse power slightly less than 1/3. This is in excellent agreement with Palmer's[10] observation that the crater depth is inversely proportional to 1/3 power of the target shear strength, and Herrmann and Jones[9] and Eichelberger's[19] observations that it is inversely proportional to the 1/3 power of the target Brinell hardness. Table IV favors an inverse dependence on K_t to a power slightly greater than 1/2 when it is used as the target material parameter.

QUANTITATIVE USE OF THE EMPIRICAL MODEL

The primary aim of this study was to provide at least first approximation formulae by which penetration into various materials might be predicted. Certainly an accuracy of 90% is better than a first approximation.

The tables of data are all collected in Appendix B to facilitate their use. Each group of tables is preceded by the appropriate distribution of target materials as a function of velocity to indicate generally the limits of applicability. It should be pointed out that, although the dependent variable is expressed in nondimensional form, the independent variables are not in nondimensional groupings. Therefore, the constants k_o will have odd sets of units which depend upon the independent variables used and their specific units. For this reason, Table XIV is included to give the material

12

parameters used in this study in their <u>proper units</u> for insertion into any of the empirical formulae.

For example, the "low" velocity relationship yielding the highest correlation becomes (Table VI, line 4)

$$P_c/V_p^{1/3} = .172\ v^{.893}\ \rho_p^{.979}\ S_t^{-.457}\ \rho_t^{-.350}$$

when only four independent variables are used. In order to obtain a dimensionless number for the ratio of $P_c/V_p^{1/3}$, it is necessary to substitute the impact velocity in feet per second, the densities in pounds per cubic inch, and the shear strength in pounds per square inch.

Taking one shot from the Utah data (Turner, Palmer, and Grow, University of Utah <u>Technical Report UU-5</u>, August 2, 1960, page 77, line 6) where the target material is lead and the projectile material is aluminum. The experimental data gives

$$P_c = 0.154 \text{ in.} \qquad V_c = .011 \text{ in.}^3$$

$$V = 3150 \text{ ft./sec.} \quad V_p = .00347 \text{ in.}^3$$

From Table XIV

$$\rho_p = .1001 \text{ lb./in.}^3 \qquad S_t = 1800 \text{ lb./in.}^2$$

$$\rho_t = .4097 \text{ lb./in.}^3$$

Substituting these independent variables into the equation yields

$$P_c/(.00347) = .172\ (3150)^{.893}\ (.1001)^{.979}\ (1800)^{-.457}\ (.4097)^{-.350}$$

so that $\qquad\qquad P_c = 0.161 \text{ in.}$

which represents a 4.5% error when compared with the experimental penetration depth.

Using the second line of Table XV

$$V_c/E_p = .0216\ v^{-.143}\ \rho_p^{.374}\ S_t^{-.814}\ \rho_t^{-.227}$$

and the fact that $E_p = 1/2\ \rho_p\ V_p\ v^2$, the equation for crater volume becomes

13

$$V_c/V_p = .0108 \, v^{1.857} \, \rho_p^{1.374} \, S_t^{-.814} \, \rho_t^{-.227}$$

Substitution of the independent variables above yields

$$V_c = 0.013 \text{ in.}^3$$

which represents a 20% error when compared with the experimental crater volume.

It is just coincidental that a shot was chosen whose crater depth was predicted within the multiple correlation coefficient and whose crater volume was not.

It is interesting to note that the equations developed in this report may be used to analyze cratering in materials recovered from orbit, and thereby make predictions on the velocity and size of the impacting projectile. If the projectile density and the target material are known, and if the penetration depth and crater volume are measured in the recovered structure, it is possible to predict the impact velocity and projectile volume. This can be done with any degree of confidence only within the impact velocity and material density ranges covered by the experimental data.

The empirical equations succeed in cutting across impact and material parameters only as well as the experimental data has been distributed across these same parameters. However, the high degree of predictability within this data should offer encouragement for experimental work at higher impact velocities and into vastly different target materials.

DIMENSIONAL MODEL

In an effort to develop a logical set of independent variables in dimensionally correct groupings against which to test experimental data, consideration has been given to the transformation processes involved in the dissipation of the projectile kinetic energy during a hypervelocity ballistic impact. In the Third Quarterly Report[3] the following mechanisms by which the impact kinetic energy may ultimately be dissipated were discussed.*

1. Kinetic energy of the backsplashed material

2. Energy required to melt, vaporize, or otherwise dissociate projectile and target material

3. Energy emitted as electromagnetic radiation at all wavelengths

4. Energy transferred to atomic, molecular, or granular change such as the energy of recrystallization.

5. Strain energy absorbed by the solid target material

Conservation of energy would then require that the impact kinetic energy be equal to the sum of these energy dissipation terms. However, it became apparent that possibly most of the impact kinetic energy can be accounted for in terms of strain energy absorbing parameters.

Other than frictional effects which occur during the process of primary crater formation, the net work done on the target may be determined largely by the non-recoverable or permanent deformational energy absorbed by the target material. That is to say, the energy dissipated as heat, sound, electromagnetic radiation, recrystallization, etc., is essentially a result of non-reversible material deformation. Thus, the correlation of impact kinetic energy with either mechanical deformational work or the combined chemical, mechanical, acoustical, thermal, electrical, etc., energies of dissipation provides dual methods for analyzing the impact problem. Even the heat generated by viscous effects on impact cannot be dissipated, except through electromagnetic radiation, during the very short period of time over which the primary crater is formed. Since the amount of electromagnetic radiation which can take place during crater formation is small *, this heat

---

* A brief discussion of the first four terms appears in Appendix A.

merely contributes to the environment under which the target material is deformed. The majority of the backsplashed material may be due to elastic recovery which occurs after the projectile ceases to exist as a causitive force, and is thus a manner in which recoverable deformational energy is dissipated by the target. Of course, there are bound to be other considerations, such as movement of the entire target, which are assumed to be secondary in this treatment.

The idea that non-recoverable strain energy accounts for the impact kinetic energy before its dissipation in other forms is not original. Goldsmith[24] points out that two approaches have been devised to account for such non-reversible phenomena: (a) the hydrodynamic theory and (b) the theory of plastic flow. It is merely suggested here that the parameters which provide a measure of a target's ability to "stop" a projectile (and in so doing, to describe the cratering process) are appropriate compression and shear energy absorbing parameters. This approach can only be justified by: (1) the fact that no attempt is being made to predict absolute cratering (only observed variations in cratering), (2) the fact that static or quasi-static material parameters are generally indicative of behavior under vastly different conditions as discussed previously under General Aspects of Target Behavior. There are, of course, discrepancies involved in the use of static or quasi-static material parameters, but these difficulties are unavoidable regardless of the method of analysis.

The problem of bridging the gap between lower velocity and hyper-velocity ballistic impact theory requires an explanation of how the projectile moving into a target with an initial velocity greater than that of any stress wave that can be detached affects the cratering process. One point that seems evident, however, is that in both cases, the cratering process depends largely on the target's ability to absorb energy which must be related in some way to pertinent impact and material parameters. If the relations governing the pressures developed in subsonic and hyper-velocity impacts constitute the primary difference in the two cases, it is shown in the discussion of Eqs. (14, 22, and 24) that the subsonic pressures, determined from the Bernoulli relation (Eq. (14)) and the hyper-velocity shock pressures, determined from one-dimensional shock theory (Eq. (22)), yield similar penetration expressions in all but possibly extremely high velocity impacts.

In order to study the behavior of the target during the impact process, it is necessary to consider the nature of the loading and the state of the material. The ordinary use of the terms solid and fluid seem to be insufficient in describing the target material under such high strain rates and pressures, etc. The hydrodynamic theory assumes that the target material has been stressed far beyond its strength and therefore behaves as a liquid with virtually no shear strength. However, since extremely high pressures tend to congeal liquids, the high pressures

produced during impact may be a result of the quasi-solid target material's ability to develop such high pressures following impact. Also, high pressures are known to substantially increase shear strengths so that, even though some type of material flow undoubtedly takes place, the shear strain energy absorbed may be a significant factor. Regardless of the magnitude of the impact velocity, there must be a certain period at the end of the crater formation period in which material strength plays a dominant role.

The compression and shear strain energy absorbed in the impact process depend generally on the following factors:

1. The magnitude and distribution of the pressures that the target material develops under the impact conditions along with the rate at which the high initial pressures are attenuated.

2. The compressibility of the target material or its reciprocal, the ability of the material to resist compressive deformation.

3. The shear toughness of the target material under the impact conditions.

DEVELOPMENT OF MODEL

The general expressions for compression and shear strain energy absorbed for the case of a simplified hemispherical surface are:

Compression Strain Energy
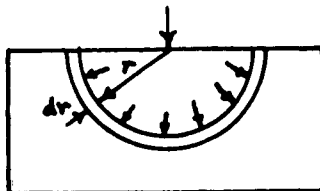
$$(E_s)_{pr} = 2\pi \int_0^{r_p} p \left(\frac{\Delta V}{V}\right) r^2 \, dr \qquad (1)$$

Shear Strain Energy

$$(E_s)_\gamma = 2\pi \int_0^{r_p} \tau \gamma r^2 \, dr \qquad (2)$$

17
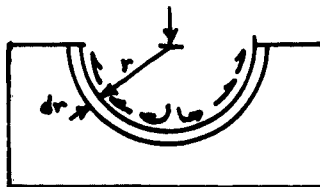
Although the extent of the inelastic deformation in the target is uncertain, it would appear to be generally a function of the target's ability to absorb compression energy. Thus, the upper limit (r_f) for the integrals might be considered as some function of the crater depth (constant times crater depth (P_C) for linear function).

A measure of the unit volume change of the target material, which appears in Eq. (1), might be taken from hydrostatic compressibility data which has been obtained for a few materials. An expression of the form

$$\frac{\Delta V}{V} = A p - B p^2 \tag{3}$$

where A and B are constants, seems to yield an empirical fit with existing data. It can be noted in Table 1 that the factor A in Eq. (3) and the compressibility (reciprocal bulk modulus) are almost identical, hence

$$\frac{\Delta V}{V} = \frac{1}{K} p - B p^2 \tag{4}$$

It is quite obvious that Eq. (4) is not really applicable to very high velocity impacts. Although the second order term is a small correction to the first order term up to a few hundred atmospheres, at a million atmospheres the two terms are roughly equal. Beyond a million atmospheres, Eq. (4) would predict an increase in volume with pressure. Dropping the second order term to form

$$\frac{\Delta V}{V} = \frac{1}{K} p \tag{5}$$

certainly does not fit the physical boundary conditions even at a few hundred atmospheres. Obviously, the hugoniot relationship developed for a given equation of state should be used here, but this introduces additional unknowns. It should be re-emphasized that the present model is only dimensional and that no attempt is being made for a self-consistent theory.

The manner in which the pressure (p) varies as a function of crater depth (r) is not known. However, if the assumption is made that the pressure varies linearly from some original pressure p_0 at the instant of impact (r = 0) to a final pressure of zero when the crater is fully formed

$$p = p_0 \frac{P_c - r}{P_c} \tag{6}$$

Then Eq. (1) may be integrated to yield

$$(E_s)_{pr.} = C_1 \frac{p_0}{K_t} P_c^3 + C_2 B p_0^3 P_c^3 \tag{7}$$

when Eqns. (4) and (6) are used, or

$$(E_s)_{pr} = C_1 \frac{P_i^2}{K_t} P_c^3 \tag{8}$$

when Eqns. (5) and (6) are used .... C_1 and C_2 are constants.

Considering the shear toughness of the crater material to be the product of S and g and the plastic shear strain in the vicinity of the final crater boundary to be a function of this toughness factor; also assuming the extent of the inelastic shear strain into the target to be some linear function of the crater depth, a solution of Eq. (2) is

$$(E_s)_\tau = C_3 (S_g)_t P_c^3 \tag{9}$$

where C_3 is a constant.

Equating the impact kinetic energy to the sum of Eqns. (8) and (9) yields

$$E_p = \frac{1}{2} \rho_p V_p v^2 = P_c^3 \left[C_1 \frac{P_i^2}{K_t} + C_3 (S_g) \right] \tag{10}$$

or

$$\frac{V_c}{E_p} = \frac{1}{C_4 P_i^2 / K_t + C_5 (S_g)_t} \tag{11}$$

where C_4 and C_5 are new constants and $V_c = \frac{2}{3} \pi P_c^3$ (hemispherical crater)

As soon as the impacting materials begin to deform, the maximum developable pressure might be considered as the dynamic fluid pressure (or stagnation pressure) for the smaller density material.

$$p = C_6 (\rho v^2) \tag{12}$$

where C_6 is a constant and ρ is the smaller of the projectile or target material density.

However, a better estimate of the pressure developed might be obtained for the case in which both projectile and target are regarded as incompressible fluids. In this case, from the Bernoulli relation,

$$p = \frac{1}{2} \rho_t v_i^2 = \frac{1}{2} \rho_p (v - v_i)^2 \tag{13}$$

where v = impact velocity
v_i = velocity of projectile-target interface

From Eq. (13),

$$(v - v_i) = \frac{\sqrt{\rho_t}}{\sqrt{\rho_p}} v_i$$

or

$$v_i = \frac{\sqrt{\rho_p}}{\sqrt{\rho_p} + \sqrt{\rho_t}} v$$

Hence,

19

or

$$p = \tfrac{1}{2}\rho_i v_i^2 = C_7 \frac{\rho_p \rho_t}{(\sqrt{\rho_p} + \sqrt{\rho_t})^2} v^2$$

$$p = C_7 \rho_{p-t} v^2 \tag{14}$$

where C_7 is a constant and ρ_{p-t} refers to a composite projectile-target density term defined as

$$\rho_{p-t} = \frac{\rho_p \rho_t}{(\sqrt{\rho_p} + \sqrt{\rho_t})^2} \tag{15}$$

Interesting comparisons are made on Lines 5 and 6 of Table 1 which show the variation of the composite density term with the projectile and target densities. Note that when the projectile and target densities are equal, the composite density term is 0.25 times either one.

   Alternately, the initial contact pressure might be determined by one-dimensional shock theory. The conservation of mass and momentum equations are written for a stationary shock front, where the undisturbed condition (ahead of the shock) and the compressed condition (behind the shock) are denoted by the subscripts 0 and 1, respectively.

Conservation of Mass
$$\rho_1 (u - v_1) = \rho_0 (u - v_0)$$

$$\tag{16}$$

Conservation of Momentum
$$(p_1 - p_0) = \rho_0 (u - v_0)(v_1 - v_0)$$

where u is the shock velocity and v is the particle velocity.

   Solving Eq. (16) yields

$$u = v_0 \pm \sqrt{\frac{\rho_1}{\rho_0} \frac{(p_1 - p_0)}{(\rho_1 - \rho_0)}} \tag{17}$$

and

$$v_1 = v_0 \pm \sqrt{\frac{(p_1 - p_0)(\rho_1 - \rho_0)}{\rho_1 \rho_0}} \tag{18}$$

If the change in compressibility with pressure is neglected, the shock velocity (u) can be taken as the dilatational wave velocity, or

$$u = c \tag{19}$$

The appropriate expression for the dilatational wave velocity c for the case where the compressibility behavior is assumed to be linear and where the contribution of shear stiffness G is neglected (inelastic range) is

$$c = \sqrt{\frac{K}{\rho}}$$

Solving Eqs. (17), (18) and (19), following the assumption that $v_0 = 0$

20

and $\rho_0 = 0$ (corresponding to the initial impact condition) yields,

(20)

for the target $\rho_I = v_I \, c_t \, \rho_t$

and for the projectile $\rho_I = (v - v_I) \, c_p \, \rho_p$ (21)

where unsubscripted v is impact velocity. Eliminating v_1 between Eqs. (20) and (21) yields an expression for the initial interface pressure

$$\rho_I = \frac{c_p \rho_p \, c_t \rho_t}{c_p \rho_p + c_t \rho_t} \, v \qquad (22)$$

A comparison of the Bernoulli pressure (Eq. (14)) with the shock pressure (Eq. (22)) in the Discussion Section shows that similar penetration expressions are obtained in all but possibly extremely high velocity impacts.

Substituting Eq. (14) for ρ_0 in Eq. (11) yields

$$\frac{V_c}{E_p} = \frac{1}{a_1 \frac{1}{K_t} \rho_{p-t}^2 \, v^4 + a_2 (sg)_t} \qquad (23)$$

Also substituting Eq. (14) for ρ_0 in Eq. (10) yields

$$\frac{P_c}{V_p^{1/3}} = \frac{\rho_p^{1/3}}{\left[a_3 \frac{1}{K_t} \rho_{p-t}^2 \, v^2 + a_4 (sg)_t \, v^{-2} \right]^{1/3}} \qquad (24)$$

The use of Eq. (7) rather than Eq. (8) in the development would result in

$$\frac{V_c}{E_p} = \frac{1}{a_1 \frac{1}{K_t} \rho_{p-t}^2 \, v^4 - a_5 \, B_t \, \rho_{p-t}^3 \, v^6 + a_2 (sg)_t} \qquad (23a)$$

and

$$\frac{P_c}{V_p^{1/3}} = \frac{\rho_p^{1/3}}{\left[a_3 \frac{1}{K_t} \rho_{p-t}^2 \, v^2 - a_6 \, B_t \, \rho_{p-t}^3 \, v^4 + a_4 (sg)_t \, v^{-2} \right]^{1/3}} \qquad (24a)$$

The use of Eq. (22) rather than Eq. (14) in Eqns. (11) and (10) gives

$$\frac{V_c}{E_p} = \frac{1}{a_7 \frac{1}{K_t} \left(\frac{c_p \rho_p \, c_t \rho_t}{c_p \rho_p + c_t \rho_t} \right)^2 v^2 + a_8 (sg)_t} \qquad (25)$$

and

$$\frac{P_c}{V_p^{1/3}} = \frac{\rho_p^{1/3}}{\left[a_9 \frac{1}{K_t} \left(\frac{c_p \rho_p \, c_t \rho_t}{c_p \rho_p + c_t \rho_t} \right)^2 + a_{10} (sg)_t \, v^{-2} \right]^{1/3}} \qquad (26)$$

ANALYSIS OF MODEL CONSTANTS

A preliminary anlysis of the dimensional model constants was made using the Utah[11] data. These data considered a variety of target materials although only over a limited range of impact velocities around 2 Km/sec. The slope of the experimental crater volume/kinetic energy curve (V_c/E_p) from reference 11 was used as an average value for each material in Table I. The model in

Table 1. Miscellaneous Calculations

Steel Projectile* - Target Material ⟶	4140 Steel	Copper	Zinc
1. From "best fit" curves (Utah, p.14) $\frac{V_c}{E_p} =$	$0.20 \times 10^{-10} \frac{cm^3}{dyne-cm}$	0.60	0.65
2. (Line 1.) x $(0.88 \times 10^{10}$ dyne-cm) $= V_c^* =$	0.176 cm^3	0.53	0.57
3. $\rho_t =$	7.90 gm/cm^3	8.95	7.14
4. (See Eq. 15), $\rho_{p \cdot t} = \rho_p \rho_t / \sqrt{\rho_p} + \sqrt{\rho_t} =$	1.96 gm/cm^3	2.11	1.86
5. $\rho_{p \cdot t} / \rho_t$ = (Line 4.)$/\rho_t$ =	0.25 dimensionless	0.24	0.26
6. $\rho_{p \cdot t} / \rho_p$ = (Line 4.)$/\rho_p$ =	0.25 dimensionless	0.27	0.24
7. (The steel value was given for iron, but value also good for steel) $K_t =$	1.67×10^{12} dyne/cm^2	1.33	0.57
8. Compressibility: $1/$(Line 7.) $= 1/K_t =$	0.600×10^{-12} cm^2/dyne	0.752	1.76
9. (Line 8.) x (980) $= 1/K_t =$	0.589×10^{-9} cm^2/gm	0.737	1.722
10. [Parameters for Eq. (3), $A_t =$	0.584×10^{-9} cm^2/gm	0.732	
11. $\frac{\Delta V}{V} = A_p - B_p^2$] $B_t =$	0.040×10^{-17} cm^4/gm^2	0.27	
12. $S_t =$	55.0×10^8 dyne/cm^2	15.8	13.1
13. Values for g could not be found. Tensile elongation values were used. Both provide a relative measure of ductility. $g_t =$	0.17 dimensionless	0.20	0.15
Calculations:			
14. $\frac{V_c}{E_p} \frac{1}{K_t} \rho_{p \cdot t}^2 v^4$ =	0.074 dimensionless	0.322	0.63
15. $\frac{V_c}{E_p} S_t$ =	0.1100 dimensionless	0.0948	0.08
16. $\frac{V_c}{E_p} (Sg)_t$ =	0.0187 dimensionless	0.0190	0.01
17. (See Eq.27), Const. $= 1/\frac{V_c}{E_p} S_t$ =	9.1 dimensionless	10.5	11.7
18. (See Eq.28), Const. $= 1/\frac{V_c}{E_p} (Sg)_t$ =	5.4 dimensionless	5.3	7.8

* For $\rho_p = 7.80$ gm/cm^3 , $V_p = 0.0564$ cm^3 , $v = 2$ Km/sec ; $E_p = \frac{1}{2} \rho_p V_p v^2 = 0$

⬤ Maximum Deviation From Mean Value.

1

Table 1. Miscellaneous Calculations

.terial ⟶	4140 Steel	Copper	Zinc	Magn.	Alum.	Lead	Reference
p.14) $\frac{V_c}{E_p}$ =	0.20×10^{-10} $\frac{cm^3}{dyne-cm}$	0.60	0.65	0.84	1.67	4.25	Utah [11]
-cm) = V_c^* =	0.176 cm³	0.53	0.57	0.74	1.47	3.74	Calculated
ρ_t =	7.90 gm/cm³	8.95	7.14	1.74	2.70	11.4	Physics Handbook [25]
$+\sqrt{\rho_t}$ =	1.96 gm/cm³	2.11	1.86	0.776	1.07	2.33	Calculated
=	0.25 dimensionless	0.24	0.26	0.44	0.40	0.20	Calculated
=	0.25 dimensionless	0.27	0.24	0.10	0.14	0.30	Calculated
or iron, K_t =	1.67×10^{12} dyne/cm²	1.33	0.57	0.34	0.75	0.44	Kent Handbook [26]
.) = $1/K_t$ =	0.600×10^{-12} cm²/dyne	0.752	1.76	2.94	1.33	2.28	Calculated
= $1/K_t$ =	0.589×10^{-9} cm²/gm	0.737	1.722	2.89	1.305	2.23	Calculated
A_t =	0.584×10^{-9} cm²/gm	0.732			1.334	2.37	Nadai, [27]
B_t =	0.040×10^{-17} cm⁴/gm²	0.27			0.35	1.73	Reinhart & Pearson [28]
S_t =	55.0×10^{8} dyne/cm²	15.8	13.1	13.0	6.5	1.2	Utah [11]
lues g_t = elative	0.17 dimensionless	0.20	0.15	0.16	0.12	0.30	Metals Handbook [29] (Except ANC-5 for Steel) [30]
≈	0.074 dimensionless	0.322	0.633	0.233	0.406	8.419	
≈	0.1100 dimensionless	0.0948	0.0852	0.1092	0.1086	0.0510	
≈	0.0187 dimensionless	0.0190	0.0128	0.0175	0.0130	0.0153	
S_t ≈	9.1 dimensionless	10.5	11.7	9.1	9.2	19.6	70%⊕
$(S_g)_t$ ≈	5.4 dimensionless	5.3	7.8	5.7	7.7	6.5	22%⊙

$V_p = 0.0564$ cm³ , $v = 2$ Km/sec ; $E_p = \frac{1}{2} \rho_p V_p v^2 = 0.88 \times 10^{10}$ dyne-cm.

in Value.

the form of Eq. (23) was used.

$$\frac{V_c}{E_p} = \frac{1}{a_1 \frac{1}{K_t} \rho_{p-t}^2 V^4 + a_2 (sg)_t} \qquad (23)$$

The various values of the quantities in Eq. (23) are shown in Table 1 along
with the appropriate reference comments. One shortcoming (noted on Line
13 of Table 1) is the necessity of using tensile elongation values instead
of ultimate shear strains g. This is not too unreasonable, however, since
both provide a relative measure of ductility. The ultimate shear strains
for the different target materials could not be found.

The Utah report [11] showed an approximate correlation of volume/energy
with shear strength (S_t) for all target materials tested except lead.

$$\frac{V_c}{E_p} = \frac{1}{CONST. (S)_t} \qquad (27)$$

These constants are repeated on Line 17 of Table 1 where maximum devia-
tion from the mean value is 70%. Since lead is the most ductile material
of the group, the possibility of a closer correlation of volume/energy
with shear toughness is suggested as

$$\frac{V_c}{E_p} = \frac{1}{CONST. (sg)_t} \qquad (28)$$

These constants are shown on Line 18 of Table 1 where the maximum deviation
from the mean value is only 22%, using the tensile elongation parameter
for the ultimate shear strain g_t.

Rewriting Eq. (23),

$$\frac{V_c}{E_p} \frac{1}{K_t} \rho_{p-t}^2 V^4 a_1 + \frac{V_c}{E_p} (sg)_t a_2 = 1 \qquad (29)$$

or, referring to Table 1,

$$\text{(line 14) } a_1 + \text{(line 16) } a_2 = 1 \qquad (30)$$

Approximate values of $a_1 = 0.02$ and $a_2 = 60$ were found by iteration using
the Utah data. When substituted into Eq. (30), these constants yield a
maximum deviation from the mean of 20% for the different materials, as
shown below.

steel:	.074 a_1 + 0.0187 a_2 = 1.1
copper:	.322 a_1 + .0190 a_2 = 1.1
zinc:	.633 a_1 + .0128 a_2 = 0.8
magnesium:	.233 a_1 + .0175 a_2 = 1.1
aluminum:	.406 a_1 + .0130 a_2 = 0.8
lead:	8.419 a_1 + .0153 a_2 = 1.1

It is interesting to note in the above relations that the very much higher coefficient of a_1 for lead may indicate the relative importance of the density term when the impact velocity is in the vicinity of the target dilatational wave velocity (the case only for lead here). The maximum impact velocities were about 2 km/sec.

OTHER MODELS

This section is adapted from the excellent paper by Herrmann and Jones for purposes of comparison and discussion. By referring to an arbitrary target resistance force F, the work-kinetic energy expression can be written as

$$\rho_p V_p \, \nu \, d\nu = -F \, dP_c \tag{31}$$

which can be integrated to yield a penetration expression for a given definition of F. This approach, however, does not intuitively include any work done on the target in the form of shear deformation.

Virtually any power expression of the form

$$\frac{P_c}{V_p^{1/3}} = C \, \rho_p^b \, \nu^d \tag{32}$$

can be obtained from Eq. (31) by assuming the resistance force to be of the form

$$F = C_1 \left(P_c^f, V_p^h, \rho_p^i, \nu^l \right)$$

where $l \neq +2$ ($l = +2$ yields a logarithmic relation). For example, if the resistance force is assumed to be proportional to penetration, as

$$F = C_2 \, P_c^2$$

or proportional to all four parameters, as

$$F = C_3 \, \frac{P_c^s}{V_p \rho_p \nu^2}$$

Eq. (31) reduces in both cases to

$$\frac{P_c}{V_p^{1/3}} = C_4 \, \rho_p^{1/3} \, \nu^{2/3} \tag{33}$$

when the constant of integration is assumed zero.

If C_4 is defined as some target material strength parameter, one possibility that provides an approximate data fit is

$$C_4 = C_5 \, H_t^{-1/3} \tag{34}$$

where the strength parameter H_t is the Brinell hardness. Eq. (33) then becomes

$$\frac{P_c}{V_p^{1/3}} = C_5 \, \frac{\rho_p^{1/3} \, \nu^{2/3}}{H_t^{1/3}} \tag{35}$$

which can be written in dimensionless form as

$$\frac{P_c}{V_p}{}^{1/3} = C_5 \left(\frac{\rho_p}{\rho_t}\right)^{1/3} \left(\frac{\rho_t \, V^2}{H_t}\right)$$

(36)

Eq. (36) can also be obtained by equating the volume/energy ratio to $H^{-1/3}$ and assuming a hemispherical crater.

A closer fit than Eq. (36) has been found by adjusting the power of the density ratio to

$$\frac{P_c}{V_p}{}^{1/3} = a_7 \left(\frac{\rho_p}{\rho_t}\right)^{2/3} \left(\frac{\rho_t \, V^2}{H_t}\right)^{1/3}$$

(37)

This expression involving both density and strength terms was shown by Herrmann and Jones to provide the best power function fit for a variety of target and projectile materials (a_7 about 0.36), although still over a somewhat limited range of impact velocities.

If now the resistance force F is assumed to be dependent on the inertia forces exerted by the target,

$$dF = (dm)a = (Area \quad ds \quad \rho_t) \frac{dv}{dt}$$

$$= C_6 \, V_p{}^{2/3} v \, dt \, \rho_t \, \frac{dv}{dt}$$

$$= C_6 \, V_p{}^{2/3} \rho_t \, v \, dv$$

(38)

and

$$F = \frac{1}{2} C_6 \, V_p{}^{2/3} \rho_t \, V^2$$

(39)

which when substituted into Eq. (31) yields upon integration

$$\frac{P_c}{V_p}{}^{1/3} = C_7 \frac{\rho_p}{\rho_t} \, \ln V + C_8$$

(40)

If C_8 is interpreted as a material strength parameter, independent of velocity, another expression similar to Eq. (39) might be written as

$$F = C_9 \, V_p{}^{2/3} (\rho_t \, V^2 + C_{10} \, H_t)$$

(41)

which leads, instead of Eq. (40), to

$$\frac{P_c}{V_p}{}^{1/3} = \frac{1}{2C_9} \left(\frac{\rho_p}{\rho_t}\right) \ln \left[\rho_t V^2 + C_{10} H_t\right] + C_{11}$$

(42)

Assuming the constant C_{11} to be zero,

$$\frac{P_c}{V_p}{}^{1/3} = \frac{1}{2C_9} \left(\frac{\rho_p}{\rho_t}\right) \ln \left[1 + \frac{1}{C_{10}}\left(\frac{\rho_t \, V^2}{H_t}\right)\right]$$

(43)

Eq. (43) was written by Herrmann and Jones as

$$\frac{P_c}{V_p}{}^{1/3} = C_{11} \left(\frac{\rho_p}{\rho_t}\right) \ln \left[1 + \frac{1}{C_{13}}\left(\frac{\rho_t \, V^2}{H_t}\right)\right]$$

(44)

where $C_{10} H_t$ multiplier (a constant for a given material) was deleted. From

27

Eq. (44), a least squares fit of existing experimental data to an equation of the form

$$\frac{P_c}{V\rho^{1/3}} = C_{12} \, \ell n \left[1 + \frac{1}{C_{13}} \left(\frac{\rho_t \, V^2}{H_t} \right) \right] \tag{45}$$

determined a more appropriate expression than Eq. (44) to be

$$\frac{P_c}{V\rho^{1/3}} = a_6 \left(\frac{\rho_\rho}{\rho_t} \right)^{1/2} \ell n \left[1 + \frac{1}{a_7} \left(\frac{\rho_\rho}{\rho_t} \right)^{2/3} \left(\frac{\rho_t \, V^2}{H_t} \right) \right] \tag{46}$$

which can be approximated by the expression

$$\frac{P_c}{V\rho^{1/3}} = C_{14} \left(\frac{\rho_\rho}{\rho_t} \right)^{0.72} \left(\frac{\rho_t \, V^2}{H_t} \right)^{1/3} \tag{47}$$

for a velocity range limited to medium and moderately high impact velocities. Eq. (47) compares very closely with Eq. (37).

The logarithmic expression involving both density and strength terms has been shown by Herrmann and Jones to fit experimental data over the entire <u>experimental</u> range, but only when appropriate values for the constants are used for given target and projectile materials. These constants were found to <u>vary widely</u> between materials.

DISCUSSION AND COMPARISON WITH EXPERIMENTAL DATA

The dimensional model was checked against the experimental data using the second "low" velocity distribution (Fig. 2)* and the "high" velocity distribution (Fig. 3)*. The least squares values of the constants (a_i) in Eqs. (24), (25), and (26) were evaluated on the digital computer. In addition, the multiple correlation coefficients (mcc) between the independent and dependent variables taken as a whole were computed for each equation. The results were as follows:

Using the second "low" velocity distribution

for Eq. (24)	$a_3 = -1.02$	$a_4 = 24.1$	mcc = -0.057
for Eq. (25)	$a_7 = -1.06 \times 10^{-3}$	$a_8 = 1.92$	mcc = -0.067
for Eq. (26)	$a_9 = -0.115$	$a_{10} = 27.5$	mcc = -0.080

Using the "high" velocity distribution

for Eq. (24)	$a_3 = 2.97 \times 10^{-4}$	$a_4 = 10.2$	mcc = 0.019
for Eq. (25)	$a_7 = 6.07 \times 10^{-4}$	$a_8 = 1.92$	mcc = 0.339
for Eq. (26)	$a_9 = 2.86 \times 10^{-5}$	$a_{10} = 10.3$	mcc = 0.003

*Appendix B

28

The a_i are not dimensionless and their units may be determined from the units of the independent variables as listed in Table XIV*.

The multiple correlation coefficients are all quite small indicating that none of the equations are doing a good job of predicting penetration over either of the velocity ranges. The negative correlation coefficients merely indicate that penetration goes down as at least one of the independent variables (probably velocity) goes up. However, since the correlation coefficients are so small, it is neither surprising nor significant that some are negative.

The least squares constants a_i when substituted into their proper equations, make the first term in the denominator negligible in comparison with the second, especially for the "high" velocity data. If, for example, the first term in the denominator of Eq. (24) is neglected, the resulting equation

$$\frac{P_c}{V_p^{1/3}} = \frac{1}{a_4} \, \mathcal{U}^{2/3} \rho_p^{1/3} \, (S_g)_t^{-1/3}$$

compares favorably with the exponents given on the fifth line of Table XIII in all but the exponent of projectile density.

At the same time an attempt was made to obtain a least squares value for the constant c_5 in the form of the Herrmann and Jones[9] equation given by Eq. (36). This attempt met with complete failure since the constant seemed to vary randomly as more and more experimental data points were added. Multiple correlation coefficients calculated using a c_5 of the order of magnitude predicted by the computer were very low. Both the Dimensional Model and the Herrmann and Jones equation suffer by comparison with the Empirical Model in that they do not leave enough constants to be evaluated by least squares.

---

*Appendix B

SUMMARY OF RESULTS AND CONCLUSIONS

The following is a brief summary of the areas investigated and the results obtained in the study of target penetration prediction by high speed and ultra high speed ballistic impact.

1. Existing experimental data relative to ballistic impact was evaluated on a statistical basis using a digital computer.

2. The limitations of present data and experimental procedures were discussed and areas for future experimental work were delineated.

3. On the basis of the statistical study, engineering formulae were developed which will predict with an accuracy of 90%,

(a) the depth of penetration

(b) the volume of the crater

in semi-infinite targets of common metals over a wide range of impact velocities. The application of these equations in predicting the size and velocity of projectiles impacting orbital structures is also indicated.

4. "Strength" parameters in general (at least for ultimate strength, shear strength, yield strength and Brinell hardness which were tested in the study) were found to be statistically indistinguishable in empirically explaining penetration behavior.

5. A general study of material behavior under static and relatively low strain-rate loading and under conditions of high speed ballistic impact was made. Qualified justification was given for the use of static or quasi-static material parameters in empirical and semi-empirical analyses of high speed impacts.

6. A dimensional penetration model was developed from a work-energy consideration which suggests that the nonrecoverable target compression and shear strain energies account for most of the kinetic energy of the projectile.

7. For limited ranges of impact velocity, the dimensional model, involving both compressibility and shear toughness parameters, was shown to yield consistent results. However, when extended to include the entire range of "experimental" velocities, and for a variety of projectile and target materials, the predominant parameter proved to be the shear-strain energy absorbing (shear toughness) parameter, for which the correlations obtained are believed to be significant.

BIBLIOGRAPHY

1. Hayes International Corp., "Study of Target Penetration Prediction By High Speed and Ultra High Speed Ballistic Impact - First Quarterly Report", October 31, 1961.

2. Hayes International Corp., "Study of Target Penetration Prediction By High Speed and Ultra High Speed Ballistic Impact - Second Quarterly Report", APGC-TDR-62-11, February 1962.

3. Hayes International Corp., "Study of Target Penetration Prediction By High Speed and Ultra High Speed Ballistic Impact - Third Quarterly Report", April 1962.

4. Hayes International Corp., "Study of Target Penetration Prediction By High Speed and Ultra High Speed Ballistic Impact - Fourth Quarterly Report", APGC-TDR-62-51, August 1962.

5. Hayes International Corp., "Study of Target Penetration Prediction By High Speed and Ultra High Speed Ballistic Impact - Fifth Quarterly Report", October 1962.

6. Bjork, R. L. Third Symposium on Hypervelocity Impact Vol. II (1959)p.35.

7. Kinard, Lambert, Schryer, and Casey, "Effect of Target Thickness on Cratering and Penetration of Projectiles Impacting at Velocities to 13,000 Feet Per Second", NASA Memo 10-18-58L, December 1958.

8. Hopkins and Kolsky, "Mechanics of Hypervelocity Impact of Solids", Hypervelocity Impact - Fourth Symposium, Vol. 1 (1960) paper #12.

9. Herrmann and Jones, "Survey of Hypervelocity Impact Information", M.I.T. - A.S.R.L. Report No. 99-1, September 1961.

10. Palmer, E. P., "Penetration and Cratering", University of Utah Technical Report UU7, October 13, 1961.

11. Johnson, Cannon, Palmer and Grow, "Cratering Produced in Metals by High-Velocity Impact", University of Utah Technical Report UU4, July 31, 1959.

12. Helie, F., Portions of "Traite de Ballistique Experimentale", translated by J. S. Rinehart, NOTS Tech. Memo RRB-75, May 1, 1950.

13. Summers, J. L., and A. C. Charters, "High Speed Impact of Metal Projectiles in Targets of Various Materials", Third Hypervelocity Symposium (1959) pg. 101.

14. Van Fleet, Partridge and Cannon, "The Anomalour Behavior of Lead-to-Lead Impacts", Third Hypervelocity Symposium (1959) p. 115.

15. Kineke, J. H., Jr., "An Experimental Study of Crater Formation in Lead", Third Hypervelocity Symposium (1959) p. 157.

16. Atkins, W. W., "Hypervelocity Penetration Studies", Third Hyper-Velocity Symposium (1959) p. 199.

17. McKenzie, Martin, Kenworthy, "High Velocity Impact of Small Metal Spheres Upon Flat Metal Targets", Third Hypervelocity Symposium (1959) p. 247.

18. Palmer, Grow, Johnson, and Turner, "Cratering Experiment and Theory", Fourth Hypervelocity Symposium, Vol. I (1960) paper #13.

19. Eichelberger, R. J. and J. W. Gehring, "Effects of Meteoroid Impacts on Space Vehicles", BRL Report No. 1155, December 1961.

20. Kineke, J. H., Jr., "An Experimental Study of Crater Formation in Metallic Targets", Fourth Hypervelocity Symposium, Vol. I (1960), paper #10.

21. Atkins, W. W., "Hypervelocity Penetration Studies", Fourth Hyper-velocity Symposium, Vol. I (1960) paper #11

22. Culp, F. L., "Volume-Energy Relation for Crater Formed by High Velocity Projectiles", Third Hypervelocity Symposium (1959) p.141.

23. Gehring, J. W., Jr., "Observations of the Phenomena of Hypervelocity Impact", Fourth Hypervelocity Symposium, Vol. II (1960) paper #29.

24. Goldsmith, W., Impact - The Theory and Physical Behavior of Colliding Solids, Edward Arnold Ltd., London (1960).

25. American Inst. of Physics Handbook, McGraw-Hill Book Co., New York, 1957.

26. Kent, William, Kent's Mechanical Engineer's Handbook, John Wiley and Sons, New York, 1956.

27. Nadai, A., Theory of Flow and Fracture of Solids, McGraw-Hill Book Co., New York, 1950.

28. Rinehart, J. S., and Pearson, J., Behavior of Metals Under Impulsive Loads, American Society for Metals, Cleveland, Ohio, 1954.

29. Metals Handbook, The American Society for Metals, Novelty, Ohio, 1948.

30. Military Handbook, MIL-HDBK-5, "Strength of Metal Aircraft Elements", Armed Forces Supply Support Center, Wash., D. C., March 1959.

31. Bruce, E. P., "Review and Analysis of Hypervelocity Impact Data", G. E. MSVD Report No. 60SD455, Sept. 29, 1960.

APPENDIX A - SOME METHODS OF ENERGY DISSIPATION

The following are some general comments on four ways by which the impact kinetic energy may eventually be dissipated by the target.

1. Kinetic energy of the material backsplashed during cavity formation

   $$E_B = (1/2\ mv^2)\ \text{backsplash}$$

   Various opinions have been expressed as to the relative magnitude of the kinetic energy of this ejected material. It does appear that the mass of the backsplash material is usually much greater than that of the original projectile. Although the Utah group[15] has measured very high velocities (up to 20 times the impact velocity for micron-sized spray particles), the average velocity of the backsplashed material must be quite small. This is verified by photographs of impacts which show large chunks of material moving backward from the point of impact with very small velocities.

2. Energy required to melt, vaporize or otherwise dissociate projectile and target material during the crater formation. It is considered of little consequence here that the actual mechanism of material separation is at least in part a result of cavitation following the disappearance of the projectile. Bromberg has pointed out that the terminal ballistic data of Summers and Charters[5] can be explained using the heat of fusion.

   $$E_L = V_c\ \rho_t\ L_t + V_p\ \rho_p L_p$$

   If any vaporization takes place, it could account for a very large portion of the impact kinetic energy. A simple calculation for an aluminum projectile striking an aluminum target at an impact velocity of 9 km./sec. shows that it would take 1/5 of the impact kinetic energy to vaporize the projectile. If the crater volume were 57 times the projectile volume (not an unreasonable figure) the energy necessary to vaporize the entire crater would be over 10 times the impact kinetic energy. The vaporization term has been eliminated from equation shown above because it appears that only a small portion of the projectile is actually vaporized. To create the spray of

micron-size, backsplashed particles being studied by the Utah[15] group would require at least a portion of the vaporization energy, but here again, the total mass of this material is small.

3. The energy emitted by electromagnetic radiation at all wavelengths due to the heat generated at the point of impact. If the absolute temperature (T) of the emitting surface were constant over an area (A) of the target, this radiant energy would be given by the Stefan-Boltzmann law as

$$E_R = e \, \sigma \, T^4 \, A \, t$$

where (e) is the emissivity, (σ) is the Stefan-Boltzmann constant, and t is the total time during which emission takes place.

The insignificance of this term can be illustrated by taking a simplified example. Consider an aluminum projectile, 0.64 centimeter diameter, impacting at 5 kilometers per second. A reasonable ratio of crater to projectile volume at this velocity would be 18. If the crater rim area is taken as the emitting area and the crater is assumed to be hemispherical, then A = 3.14 square centimeters. Taking the time over which radiation takes place to be the upper limit of the time for full crater formation (t $\approx$ 100 microseconds), the temperature necessary to yield a ratio of $E_R/E_p = 1/1000$ would be about 10,000°K.

4. Energy transferred to atomic, molecular, or granular change such as the energy of recrystallization

$$E_A = ?$$

The Utah[10] group has shown that from 12 to 15% of the energy required to push a lead ball into a lead target quasi-statically goes into recrystallization. It has not yet been determined what independent variables might enter into this term.

APPENDIX B
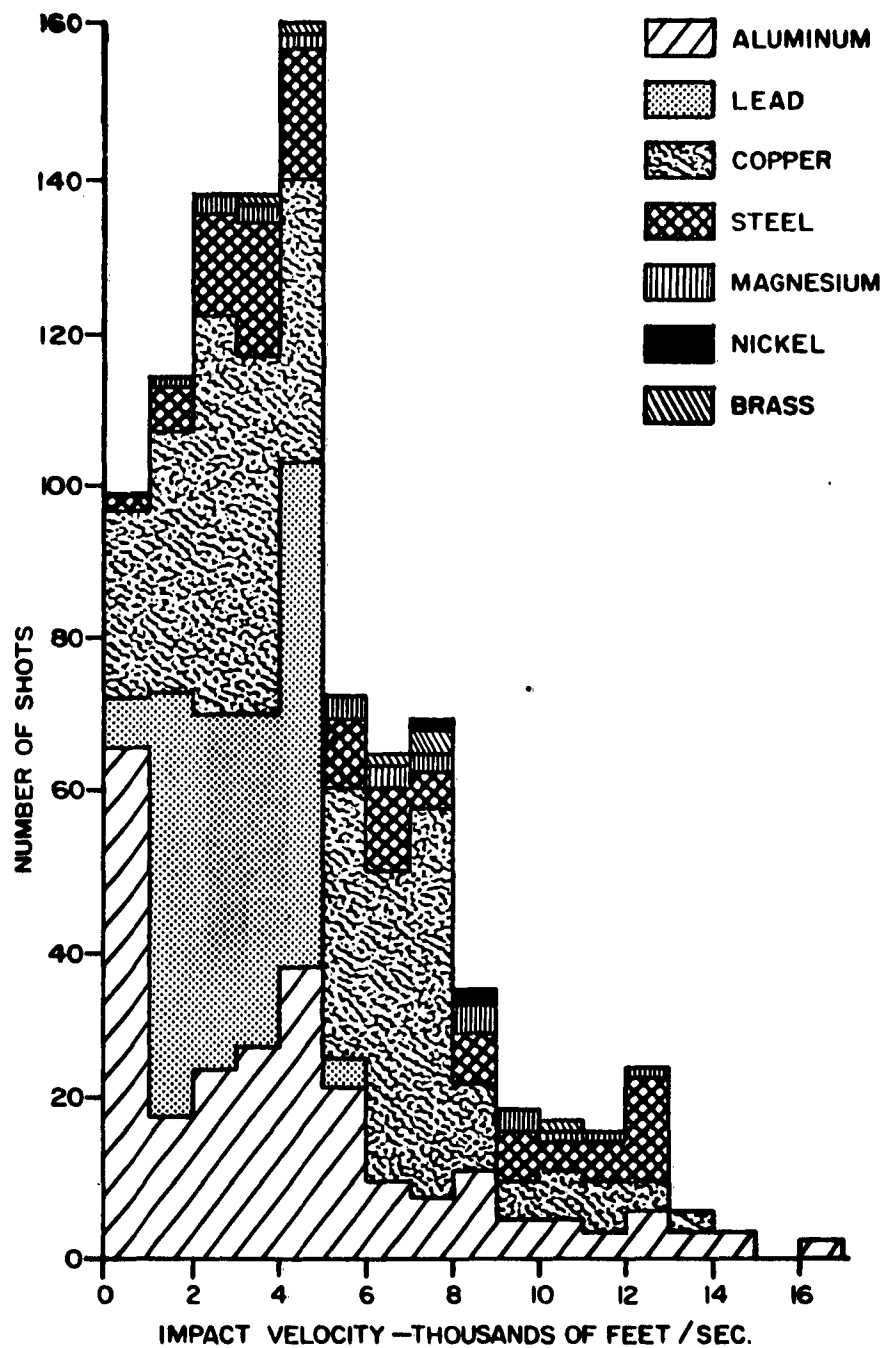
TABULATED DATA FROM THE EMPIRICAL MODEL

Figure 1. First "Low" Velocity Distribution of Target
Materials as a Function of Impact Velocity
985 Shots

36

Table I. First "Low" Velocity Data Evaluation of the Coefficients k_i in the Equation

$$P_{c/D_p} = k_o v^{k_1} \rho_t^{k_2} \rho_p^{k_3} C_t^{k_4} T_t^{k_5} e_t^{k_6} V_p^{k_7}$$

k_o	k_1	k_2	k_3	k_4	k_5	k_6	k_7	Multiple Correlation Coefficient
34.4	1.01	-.578	.969	-1.26	.575	.177	.0229	.829
36.3	.995	-.610	.959	-1.28	.548	.192		.827
173	.963	-.571	.959	-1.35	.613			.823
151	.949	-.515	.988	-1.27				.812
5.45×10^{-3}	.808	.158	.848					.695
7.64×10^{-3}	.649	.283						.532

37

Table II. First "Low" Velocity Data Evaluation of the Coefficients k_I in the Equation

$$P_{c/D_p} = k_o v^{k_1} \rho_t^{k_2} \rho_p^{k_3} H_t^{k_4} T_t^{k_5} e_t^{k_6} V_p^{k_7} C_t^{k_8}$$

k_o	k_1	k_2	k_3	k_4	k_5	k_6	k_7	k_8	Multiple Correlation Coefficient
1.21×10^{-3}	1.07	-.294	.951	-.293	.398	.279	.033	.316	.846
0.11×10^{-3}	1.08	-.186	.939	-.366	.329	.320	.036		.845
0.12×10^{-3}	1.06	-.224	.921	-.366	.277	.350			.839
0.46×10^{-3}	.993	-.090	.910	-.380	.363				.825
4.00×10^{-3}	.988	-.078	.932	-.376					.821
5.45×10^{-3}	.808	.158	.848						.695

Table III. First "Low" Velocity Data Evaluation of the Coefficients k_i in the Equation

$$P_c/D_p = k_o v^{k_1} \rho_t^{k_2} \rho_p^{k_3} S_T^{k_4} T_t^{k_5} e_t^{k_6} v_p^{k_7} C_t^{k_8}$$

k_o	k_1	k_2	k_3	k_4	k_5	k_6	k_7	k_8	Multiple Correlation Coefficients
8.43×10^{-3}	1.06	-.365	.984	-.400	.586	.010	.035	.252	.846
1.99×10^{-3}	1.07	-.298	.983	-.478	.571	-.012	.038		.845
2.19×10^{-3}	1.04	-.338	.963	-.476	.515	.021			.838
2.39×10^{-3}	1.04	-.333	.963	-.480	.522				.838
4.97×10^{-3}	1.03	-.364	.991	-.464					.831
5.45×10^{-3}	.808	.158	.848						.695

39

Table IV. First "Low" Velocity Data Evaluation of the Coefficients k_i in the Equation

$$P_{c/D_p} = k_o \, v^{k_1} \, \rho_t^{k_2} \, \rho_p^{k_3} \, K_t^{k_4} \, T_t^{k_5} \, e_t^{k_6} \, v_p^{k_7} \, c_t^{k_8}$$

k_o	k_1	k_2	k_3	k_4	k_5	k_6	k_7	k_8	Multiple Correlation Coefficient
1.95	1.01	-.564	.970	-.019	.575	.169	.022	-1.23	.829
.634	.935	.028	.993	-.510	.405	.067	.014		.790
.803	.927	.015	.928	-.523	.391	.069			.789
1.40	.917	.039	.929	-.544	.414				.788
13.4	.910	.052	.952	-.531					.783
5.45×10^{-3}	.808	.158	.848						.695

Table V. Individual Correlation Coefficients Between the Variables Used in the Present Analysis (Based on First "Low" Velocity Data)

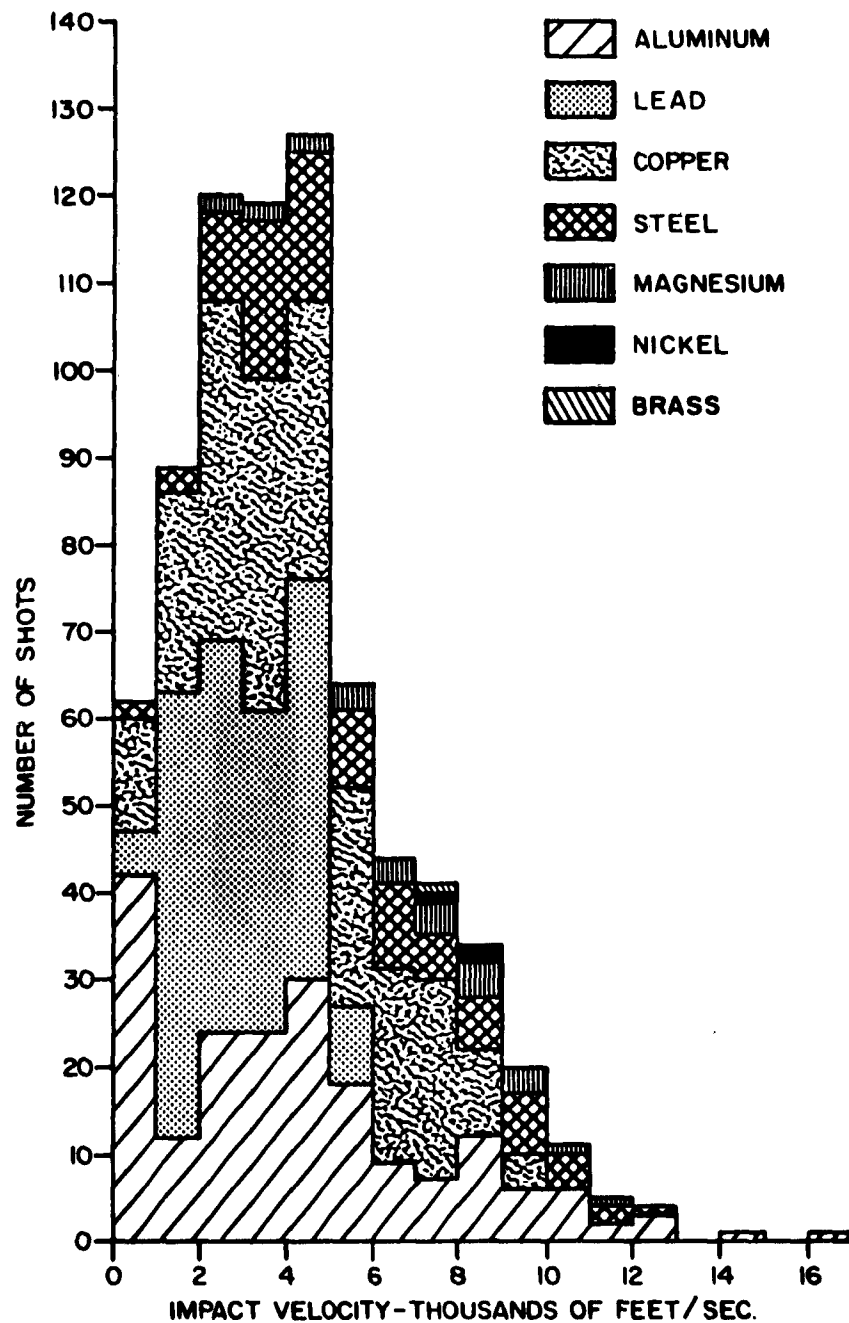|	v	ρ_t	ρ_p	T_t	C_t	U_t	Y_t	S_t	e_t	H_t	V_p	K_t
P_c/D_p	.055	.024	.053	.024	-.064	-.067	-.064	-.063	.006	-.065	.089	-.054
v		.096	-.238	-.063	.082	.238	.319	.218	.013	.241	-.204	.127
ρ_t			.142	.088	.672	-.343	-.221	-.473	.046	-.268	-.211	-.118
ρ_p				.168	-.013	.017	-.018	-.004	.019	-.016	-.095	.059
T					.078	.053	.004	.067	.004	.026	-.116	.080
C_t						.855	.769	.897	-.025	.791	.011	.535
U_t							.971	.943	-.010	.973	.036	.603
Y_t								.884	-.005	.969	-.045	.579
S_t									-.027	.891	.002	.622
e_t										-.004	-.007	-.006
H_t											.015	.557
V_p												-.120

41

Figure 2   Second "Low Velocity" Distribution of Target
Materials as a Function of Velocity - 742
Shots

Table VI. Second "Low" Velocity Data Evaluation of the Coefficients k_i in the Equation

$$P_c/v_p^{1/3} = k_o v^{k_1} \rho_p^{k_2} S_t^{k_3} \rho_t^{k_4} e_t^{k_5} K_t^{k_6} C_t^{k_7}$$

k_o	k_1	k_2	k_3	k_4	k_5	k_6	k_7	Multiple Correlation Coefficient
.0118	.879	1.01	-.437	-.326	-.006	-.036	.335	.934
.125	.897	.977	-.455	-.350	.036	.009		.925
.140	.897	.978	-.450	-.345	.036			.925
.172	.893	.979	-.457	-.350				.925
.189	.840	.915	-.379					.900
.025	.626	.825						.725

43

Table VII. Second "Low" Velocity Data Evaluation of the Coefficients k_i in the Equation

$$P_c/V_p^{1/3} = k_o \, v \, \rho_p \, C_t \, \rho_t \, e_t \, K_t \, C_p$$

k_o	k_1 v	k_2 ρ_p	k_3 C_t	k_4 ρ_t	k_5 e_t	k_6 K_t	k_7 C_p	Multiple Correlation Coefficient
3.41	.816	1.03	-2.27	-1.18	.192	.557	.415	.913
82.5	.823	.954	-1.87	-.983	.259	.373		.899
92.3	.829	.976	-1.19	-.611	.257			.898
1008	.790	.988	-1.34	-.677				.893
14.9	.708	.866	-.736					.830
.025	.626	.825						.725

Table VIII. Second "Low" Velocity Data Evaluation of the Coefficient k_I in the Equation

$$P_{c}/V_p^{2/3} = k_o\, v^{k_1}\, \rho_p^{k_2}\, H_t^{k_3}\, \rho_t^{k_4}\, e_t^{k_5}\, K_t^{k_6}\, C_p^{k_7}$$

k_o	k_1	k_2	k_3	k_4	k_5	k_6	k_7	Multiple Correlation Coefficient
.0005	.869	1.00	-.443	-.370	-.090	.004	.325	.932
.005	.887	.976	-.465	-.400	-.057	.058		.924
.013	.883	.978	-.435	-.371	-.047			.923
.010	.887	.975	-.426	-.365				.923
.019	.832	.909	-.348					.896
.025	.626	.825						.725

Table IX. Second "Low" Velocity Data Evaluation of the Coefficients k_i in the Equation

$$P_c/V_p^{\frac{1}{3}} = k_o \, v^{k_1} \, \rho_p^{k_2} \, (Se)_t^{k_3} \, \rho_t^{k_4} \, e_t^{k_5} \, K_t^{k_6} \, C_p^{k_7}$$

k_o	k_1	k_2	k_3	k_4	k_5	k_6	k_7	Multiple Correlation Coefficient
.012	.879	1.01	-.437	-.326	-.443	-.036	.335	.934
.125	.897	.977	-.455	-.350	τ.419	.010		.925
.140	.897	.978	-.450	-.345	-.414			.925
.020	.919	.955	-.365	-.287				.918
.030	.874	.906	-.317					.900
.025	.626	.825						.725

46
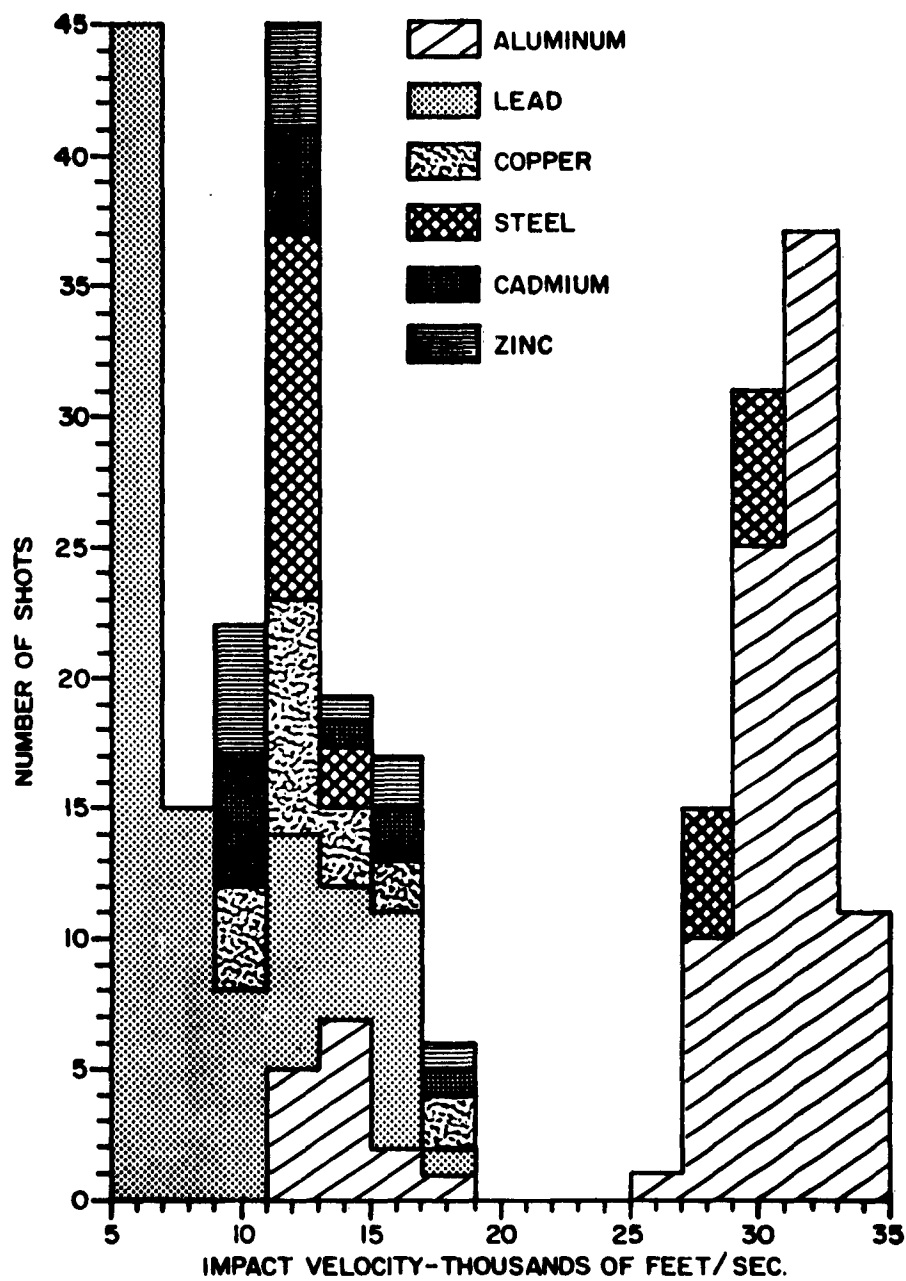
Figure 3. "High Velocity" Distribution of Target Materials
as a Function of Velocity - 266 Shots

Table X. "High" Velocity Data Evaluation of the Coefficients k_i in the Equation

$$P_c/V_P^{1/3} = k_0\ v^{k_1}\ \rho_P^{k_2}\ s_t^{k_3}\ \rho_t^{k_4}\ e_t^{k_5}\ K_t^{k_6}\ c_P^{k_7}$$

k_0	k_1	k_2	k_3	k_4	k_5	k_6	k_7	Multiple Correlation Coefficient
.328	.474	.675	-.362	-.489	-.123	.117	-.014	.877
.290	.472	.675	-.362	-.489	-.122	.117		.877
1.12	.468	.670	-.300	-.431	-.103			.875
.772	.449	.673	-.275	-.426				.874
.108	.658	.546	-.235					.817
.565	.268	.612						.644

Table XI. "High" Velocity Data Evaluation of the Coefficients k_i in the Equation

$$P_{c/V_p^{1/3}} = k_o \, v^{k_1} \, \rho_p^{k_2} \, C_t^{k_3} \, \rho_t^{k_4} \, e_t^{k_5} \, K_t^{k_6} \, C_p^{k_7}$$

k_o	k_1	k_2	k_3	k_4	k_5	k_6	k_7	Multiple Correlation Coefficient
35.2	.364	.721	-1.43	-.993	.157	.404	.013	.851
39.8	.364	.720	-1.43	-.993	.156	.405		.851
61.4	.371	.689	-.729	-.597	.137			.845
190	.383	.686	-.821	-.623				.841
2.58	.580	.534	-.494					.738
.565	.268	.612						.644

Table XII. "High" Velocity Data Evaluation of the Coefficients k_i in the Equation

$$P_c/V_p^{1/3} = k_o \, v^{k_1} \, \rho_p^{k_2} \, H_t^{k_3} \, \rho_t^{k_4} \, e_t^{k_5} \, K_t^{k_6} \, C_p^{k_7}$$

k_o	k_1	k_2	k_3	k_4	k_5	k_6	k_7	Multiple Correlation Coefficient
.017	.464	.682	-.365	-.558	-.097	.167	-.019	.875
.014	.463	.684	-.364	-.558	-.096	.166		.875
.169	.456	.675	-.278	-.463	-.071			.872
.146	.443	.677	-.262	-.458				.871
.025	.656	.543	-.215					.806
.565	.268	.612						.644

Table XIII. "High" Velocity Data Evaluation of the Coefficients k_i in the Equation

$$P_c/v_p^{1/3} = k_o v^{k_1} \rho_p^{k_2} (Se)_t^{k_3} \rho_t^{k_4} e_t^{k_5} K_t^{k_6} c_p^{k_7}$$

k_o	k_1	k_2	k_3	k_4	k_5	k_6	k_7	Multiple Correlation Coefficient
.328	.473	.674	-.362	-.489	.239	.117	.014	.877
.291	.473	.675	-.362	-.489	.240	.117		.877
1.12	.468	.670	-.300	-.431	.197			.875
2.81	.486	.663	-.340	-.426				.865
.326	.687	.537	-.288					.808
.565	.268	.612						.644

51

Table XIV. Material Parameters

Material	ρ lb/in³	S psi × 10⁴	K psi × 10⁷	H kg/mm²	e %	c ft/sec × 10⁴	v_2 ft/sec × 10²	v_3 ft/sec × 10⁴	v_4 ft/sec × 10⁴	U psi × 10⁴	Y psi × 10⁴
Al 2024 T4 ⎫ 2024 T3 ⎬ 2023 T4 ⎭	0.1001	4.10	1.04	120	20	2.05	11.2	1.67	5.01	6.8	4.7
2014 T6	0.101	4.20	1.04	135	13	2.05	12.7	1.67	5.01	7.0	6.0
1100 F	0.098	1.00	1.01	28	18	2.01	6.4	1.66	4.99	1.6	1.5
1100 O	0.098	0.90	1.01	23	40	2.01	2.67	1.66	4.99	1.12	0.26
2024 O	0.101	1.80	1.04	47	21	2.05	5.78	1.67	5.01	3.00	1.26
Steel 1030	0.283	7.17	2.33	177	16	1.79	8.49	1.49	4.46	8.35	7.60
1020	0.283	6.27	2.33	148	17.2	1.79	8.07	1.49	4.46	7.01	6.87
4140	0.283	7.98	2.33	285	16.5	1.79	9.33	1.49	4.46	14.7	9.17
Pb	0.4097	0.18	0.44	4	30	0.59	0.07	0.54	1.62	0.19	0.08
Cu (Raytheon)	0.323	2.20	1.67	45	45	1.55	2.88	1.18	3.53	3.20	1.00
pure	0.324	2.60	2.27	77	14	1.62	6.39	1.37	4.12	5.09	4.93
Mg	0.063	1.70	0.72	40	16	2.11	7.73	1.75	5.16	2.70	1.40
Zn	0.259	3.10	0.70	72	10	1.20		0.85	2.56	4.10	
Cd	0.312	0.87	0.89	24	50	1.23		0.87	2.62	1.03	
Ni	0.321	6.00	3.05	105	42	1.95	5.18	1.60	4.79	6.50	2.00
Brass	0.308	4.00	2.12	112	23	1.59	6.73	1.36	4.08	6.20	5.20

Table XV. Evaluation of the Coefficients in the Equation

$$V_c/E_p = k_o v^{k_1} \rho_p^{k_2} S_t^{k_3} \rho_t^{k_4}$$

	k_o	k_1	k_2	k_3	k_4	Multiple Correlation Coefficient
Second "Low" Velocity Data	.0216	-.143	.374	-.814	-.227	.952
"High" Velocity Data	.111	-.571	.664	-.516	-.412	.847

INITIAL DISTRIBUTION

Hq USAF (AFTAC) Washington 25, D. C.	1	Commander, ASD (ASAD-Lib) Wright-Patterson AFB, Ohio	3
Hq USAF (AFCIN-3K2) Washington 25, D. C.	1	Commander, AFSWC Kirtland Air Force Base, N. M. Attn: Technical Info Div.	2
Hq USAF (AFRDC) Washington 25, D. C.	2	Commander, AFCRL L. G. Hanscom Field Attn: CRQST-2 Bedford, Mass.	1
Hq USAF (AFRAE-E) L/C Hicks, TTCP O-1	1		
USAF: AFTST-EL/CS Maj. Myers	1	AFOSR Bldg "D" Washington 25, D. C.	1
USAF: AFRST-PM/ME Maj. Geiseman	1	AFOSR (SRHP – Dr. M. M. Slawsky) Bldg "D" Washington 25, D. C.	1
Commander AFSC Attn: SCRWA Andrews Air Force Base Washington 25, D. C.	1	AFOSR (SRHP – Dr. J. F. Masi) Bldg "D" Washington 25, D. C.	1
Commander AFSC Attn: SCTA, Mr. Robert Fisk Andrews Air Force Base Washington 25, D. C.	1	AFOSR (Dr. A. G. Horney) Bldg "D" Washington 25, D. C.	1
Commander, BSD (AFSC) Col. Brassfield Air Force Post Office Los Angeles 25, Calif.	2	AFOSR (SRHP – Dr. M. M. Slawsky) For: Rckt Pwr/Tal Div Gabriel Co) Attn: Dr. R. Reed, Jr. Washington 25, D. C.	1
Commander, ASD Attn: ASAPRL Wright-Patterson AFB, Ohio	1	AFOSR (Dr. M. M. Slawsky) For: Univ of Utah (Dr. M. A. Cook) Bldg "D" Washington 25, D. C.	1
Commander, ASD Attn: ASRMDS Wright-Patterson AFB, Ohio Attn: Mr. Philip Parmley	1	Commanding General White Sands Missile Range, N. M. Attn: ORDBS-OM-W	1

TAC (TPL-RQD-M)
Langley AFB, Va.

Director, NASA
1502 H Street, N. W.
Washington 25, D. C.   1

Director, NASA
Langley Rsch Ctr
Langley Fld, Va.
Attn: Technical Library   2

Director, NASA
Langley Rsch Ctr
Langley Fld, Va.
Attn: W. H. Kinard   1

Director, NASA
Langley Rsch Ctr
Langley Fld, Va.
Attn: Mr. John Stack   1

Director, NASA
Ames Research Center
Moffett Field, Calif.
Attn: Tech Library   4

Marshall Space Flight Center
M-AERO-TS (W. D. Mruphree)
Huntsville, Alabama   1

Marshall Space Flight Center
Advanced Research Projects Lab
Attn: Dr. William Johnson
Huntsville, Alabama   1

Director
Advanced Rsch Projects Agency
Attn: Dr. Charles Bates
Washington 25, D. C.   1

Director of Defense Research
and Engineering
Attn: Technical Library
Washington 25, D. C.   1

Director of Defense Research
and Engineering
Attn: Dr. R. M. Yates
Washington 25, D. C.   2

ARO (Scientific Info Br)
Washington 25, D. C.   2

Armour Research Foundation
10 West 35th Street
Mr. G. H. Strohmeier (Dir, Def Rsch)
Chicago 16, Illinois   1

University of Chicago
Institute for Air Wpns
Attn: Library
Chicago, Illinois   1

The Franklin Institute of the State of
Pennsylvania
Benjamin Franklin Pkwy at 20th Street
Philadelphia 2, Penn.
Attn: Technical Library   2

SSD
AF Unit PO
Los Angeles 45, Calif.   2

California Institute of Technology
Jet Propulsion Lab
Attn: Dr. W. H. Pickering
Pasadena, Calif.   1

John Hopkins University
Applied Rsch Lab
White Oak, Silver Spring, Md.   2

OAR (RROSA)
Bldg T-D
Washington 25, D. C.
Attn: Maj. E. J. Davis   1

OAR (RROSA)
Bldg T-D
Attn: Maj. George Stalk
Washington 25, D. C.   1

55

ASTIA (TIPCR) Arlington Hall Stn Arlington 12, Va.	15	Frankford Arsenal (Lib) Philadelphia 37, Penn.
Lewis Rsch Ctr Cleveland 35, Ohio	3	Frankford (Pitman-Dunn Lab) Philadelphia 37, Penn.

ASTIA (TIPCR)
Arlington Hall Stn
Arlington 12, Va.   15

Lewis Rsch Ctr
Cleveland 35, Ohio   3

Director
IDA/Wpns Sys Eval Gp
Rm 1E880, The Pentagon
Washington 25, D. C.   2

Director, Project RAND
Dept. of the Air Force
1700 Main Street
Santa Monica, Calif.
Attn: Technical Library   1

Army Materiel Command
Research Directorate
Attn: MCR
Washington 25, D. C.   3

Commanding Officer
Picatinny Arsenal (ORDBR-TK)
Dover, N. J.   2

Commanding General
Aberdeen Proving Ground, Md.
Attn: R. J. Eichelberger   1

Commanding General
Aberdeen Proving Ground
Attn: J. Kineke   1

Commanding General
Aberdeen Proving Ground, Md.
Attn: F. E. Allison   1

Redstone Scientific Info Ctr.   1
U. S. Army Missile Command
Redstone Arsenal, Alabama

Frankford Arsenal (Lib)
Philadelphia 37, Penn.   1

Frankford (Pitman-Dunn Lab)
Philadelphia 37, Penn.   1

Springfield Armory (R & D Div)
Springfield, Mass.   2

Watervliet Arsenal (ORDBR-R)
Watervliet, N. Y.   2

Watertown Arsenal
Watertown, Mass.   2

Rock Island Arsenal
Rock Island, Illinois   1

Commanding General
Engineer Rsch & Div Labs
Attn: Chief, Tech Support Br
U. S. Army, Ft Belvoir, Virginia   1

Director of Special Wpns Div
U. S. Continental Army Command
Attn: Chester I. Peterson
Fort Bliss, Texas   1

U. S. Army Research Office
Attn: Dr. A. S. Galbraith.
Duke Station
Durham, N. C.   2

Commanding General   1
Aberdeen Proving Ground, Md.
Attn: Technical Library

Chief, Bureau of Naval Weapons   4
Dept. of the Navy (R-12)
Washington 25, D. C.

Chief, Bureau of Naval Weapons Dept. of the Navy (RM) Washington 25, D. C. 4	ASQR	**2**
	PGAPI	**9**
Director U. S. Naval Research Lab Washington 25, D. C. 1 Attn: Mr. W. W. Atkins, Code 130	PGEH	**3**
	PGWR	**2**
Commanding Officer U. S. Naval Ordnance Test Station China Lake, California Code 5007 2	PGWRT	20

Commanding Officer
U. S. Naval Ordnance Test Station
China Lake, California
Attn: Technical Library   2

Commander
U. S. Naval Ordnance Lab
White Oak, Silver Spring, Md.
Attn: Technical Library   2

U. S. Naval Wpns Lab
Dahlgren, Virginia
Attn: Technical Library   2

Commander, ASD (Attn: Don Lewis, ASRNGW)
Wright-Patterson AFB, Ohio   1

OOAMA (OOYD)
Hill AFB, Utah   1

NASA   1
Office of Advanced Research (RV2)
Attn: Mr. Howard Wolko
1512-1520 H. Street N. W.
Washington 25, D. C.

Air Proving Ground Center, Eglin Air Force Base, Florida
Rpt No. APGC-TDR-63-22. STUDY OF TARGET PENETRATION PRE-
DICTION BY HIGH SPEED AND ULTRA HIGH SPEED BALLISTIC IMPACT.
Final Report, April 1963, 57 p. incl illus, 31 refs. Unclassified Report.

On the basis of a statistical study of existing experimental data relative to
ballistic impact, engineering formulae were developed which will predict
with an accuracy of 90%, (a) the depth of penetration, (b) the volume of the
crater, in semi-infinite targets of common metals over a wide range of
impact velocities. The application of these equations in predicting the size
and velocity of projectiles impacting orbital structures is also indicated.
A semi-rational penetration expression was developed from a work-energy
consideration which suggests that the nonrecoverable target compression
and shear strain energies may account for most of the kinetics energy of
the projectile. This dimensional model agrees quite well with the general
features of, and is subject to, the same limitations as existing theoretical
and empirical models.

1. Hypervelocity projectiles
2. Penetration
3. Cratering
I. OAR Project 9860
II. Contract AF 08(635)-2155
III. Hayes International Corp.,
    Birmingham, Alabama
IV. In ASTIA collection